On the seismic response of a periodic sequence of three thin layers saturated by two-phase fluids

(February 22, 2021)

Running head: **Seismic response of saturated layers**

ABSTRACT

The conversion of fast to slow diffusion P-waves in fluid-saturated porous media induces attenuation and dispersion of waves at seismic frequencies. This effect, known as wave induced fluid flow (WIFF), occurs at mesoscopic scales, which are much larger than the average pore size and much smaller than the average fast P-wave wavelength. When analyzing this mechanism in hydrocarbon reservoirs with the pore space saturated by multiphase fluids, it is important to include capillary pressure effects and flow interaction between fluids, which cause additional attenuation and velocity dispersion of P-waves. We present a procedure to determine the phase velocities and dissipation factors in a medium composed of a periodic sequence of three poroelastic thin layers saturated by two-phase fluids. The methodology consists of applying compressibility tests to representative samples of the material, which are defined as boundary-value problems solved using a finite-element (FE) procedure. First, we analyze the case of two-phase fluids saturation on each layer and the results are compared with those of the single-phase (effective) fluid case. Then, several cases of patchy saturation are presented, indicating that residual and wetting fluid saturation play an important role to determine the P-wave velocities and dissipation factors.

INTRODUCTION

Wave induced fluid flow (WIFF) is an important mechanism, responsible for the high levels of attenuation and dispersion observed at seismic frequencies in partially saturated rocks. This effect is due to mode conversions at mesoscopic-scale heterogeneities in the saturant fluids and porous frame, where the mesoscopic scale is much smaller than the predominant wavelengths but much larger than the average pore diameter. Wave propagation in poroelastic solids saturated by single-phase fluids was presented by Biot in several papers (Biot, 1956, 1962). The theory predicts the existence of two compressional modes (P1, fast and P2, slow) and one shear wave.

Biot's theory does not hold when the rock is saturated by two-phase fluids, since capillary pressure effects and interaction between flows are ignored. These effects induce changes in phase velocities and dissipation factors. To analyze this phenomenon we simulate the seismic response of a porous medium composed of a periodic sequence of three layers saturated by two-phase fluids using an extension of Biot's theory presented in several papers Santos et al. (1990a,b); Ravazzoli et al. (2003); Carcione et al. (2004). The difference between single- and two-phase fluid saturation in poroelastic media is evident in the significant changes needed in the original Biot theory (Biot, 1962) in order to consider two fluids. First, the capillary pressure is incorporated into the constitutive relations via a Lagrange multiplier in the complementary virtual-work principle. Consequently, with the exception of the shear modulus, all other elastic constants depend on the capillary pressure. Second, the dissipation function, as a quadratic function of the the relative particle velocity between the solid and fluid phases, depends on the relative permeabilities (Peaceman, 1977; Scheidegger, 1974), in addition to the absolute permeability used for single-phase fluids. The former

represent the interference between the flow of the two fluid phases as they move within the pore space.

Interfacial tensions and fluid flow interferences are included by using a phenomenological approach representing those effects as averages over representative samples of the material via capillary pressure and relative permeability functions.

The inclusion of capillary pressure and relative permeabilities at mesoscopic scales based on Santos et al. (1990a,b), induces noticeable changes in the behavior of the system as compared with the case when single-phase fluid saturation is assumed. In fact: the theory predicts the existence of three compressional waves (P1, fast, P2 and P3, slow) and one shear wave. While capillary pressure is responsible for the existence of one additional slow wave, the relative motions between the two fluid phases induce additional energy losses not present in the case of single-phase fluids. In this model, capillary pressure is assumed to be a unique function of saturation (ignoring hysteresis), while dissipative effects are modeled via the two-phase Darcy's law using relative permeability functions, also assumed to be functions of saturation. (Peaceman, 1977; Scheidegger, 1974). Since the model was derived from first principles, the equations are valid for heterogeneus materials, so that no boundary conditions are needed at interior interfaces. For additional details on the extension of Biot's theory to the case of two-phase fluids and its applications in reservoir rocks using the FE method, we refer to Santos and Gauzellino (2017) .

Based on Biot's theory, White et al. (1975) were the first to study the WIFF mechanism by analyzing the seismic response of plane layers alternately saturated with gas and water. Later, Norris (1993) implicitly extended the results for many layers and Cavallini et al. (2017) found the explicit analytical solution for three layers. This solution has been

compared with FE simulations (S. Picotti et al., personal communication, 2020).

Among other authors studying the WIFF mechanism, Ba et al. (2017) present a double-porosity model considering the rock fabric and fluid heterogeneities, and effective single-phase fluids. They observe two inflection points of the velocity and two attenuation peaks in the ultrasonic range, one caused by fabric heterogeneity and the other by patchy gas-water saturation. Their results are not related to capillary pressure effects. The peaks in our theory are of a mesoscopic (WIFF) nature, located in the seismic band, and we include the effect of interfacial tension between the fluids (realistic two-phase fluids).

Barbosa et al. (2017) and Hunziker et al. (2018) perform a numerical study of seismic attenuation and dispersion considering 2D fractured Biot media saturated by single-phase fluids with either anisotropic frame or stochastic fracture networks. They carry out compressibility and shear tests on representative samples to obtain the phase velocity and attenuation of P and S waves as a function of frequency and incidence angle. The two peaks observed by Hunziker et al. (2018) are associated with the different density and connectivity of fracture, and not to capillary pressure effects. Their differential boundary value problems (BVP's) and Finite Element (FE) are those appeared in Santos et al. (2009), where uniqueness results, a priori error estimates and appropriate selection of the computational mesh are given to represent the diffusion process. This analysis is missing in Barbosa et al. (2017) and Hunziker et al. (2018).

Rozhko (2019) investigate the effect of the hysteresis of liquid bridges on seismic attenuation and bulk moduli of a partially saturated rock. His model requires too many parameters to represent the effect of capillary pressure, not fully available in laboratory experiments. Furthermore, Rozhko (2020) extended Gassmann's formula to include capillary

pressure effects.

In any case, hysteresis occurs in drainage-imbibition experiments. Here, we assume a single capillary-pressure curve and is that of drainage, i.e., the non-wetting fluid (oil or gas) displacing the wetting fluid in a water-wet formation (imbibition is the opposite process). Drainage occurs naturally when the oil or gas migrates from the source rock into the reservoir pore volume, displacing some of the water that originally fills it and determining the initial fluid saturations found when the reservoir was discovered.

The model for capillary pressure and relative permeabilities used in this work is that of Scheidegger (1974), where the funicular regime is defined as a continuous network of both phases across the porous medium. It is thus possible that simultaneous flow of both phases occurs along what must be very tortuous (funicular) paths. See also Chavent and Jaffre (1986). This model is commonly used in numerical reservoir simulations to model two-phase fluid flow at mesoscopic scales. They include residual saturations S_{rw}, S_{rn} for the non-wetting and wetting phases, respectively, meaning immobile wetting fluid in $[0, S_{rw}]$ and immobile non-wetting fluid in $[0, S_{rn}]$, with capillary pressure tending to infinity when wetting saturation approaches S_{rw}. In hydrocarbon reservoirs $S_{rw} > 0$, with the physical meaning that an infinite amount of energy would be needed to remove the immobile wetting phase. Hysteresis may be included by taking either the drainage or imbibition branches of the capillary-pressure curve, but we do not expect significant differences in our analysis.

Pride et al. (2004) analyze seismic attenuation due to WIFF flow using a double-porosity model of a mixture of two porous solids saturated by a single-phase fluid. They study heterogeneities in the lithology, the case of patchy saturation and squirt flow, concluding that the latter can not explain the levels of attenuation observed in the seismic band. For patchy

saturation, they estimate when the capillary effects are important for fluid equilibration. The situations where both phases form continuous paths across each averaging volume (i.e. funicular regime) is not treated in this paper. Li and Horne (2004) use fractal geometry to represent capillary pressure for a type of rock that can not be represented by the model presented by Brooks and Corey (1964). They use a modified version of the Leverett function, the content is essentially in Scheidegger (1974) and Chavent and Jaffre (1986).

Wollner and Dvorkin (2016, 2018) perform numerical experiments to determine the effective fluid bulk modulus in a sequence of thin layers using Gassmann fluid substitution. They find that the effective fluid modulus is a linear combination of the saturation-weighted harmonic and arithmetic averages and depends on the hydraulic communication between adjacent layers. In our work, interlayer flow is implicit because we use a Biot's aproach modeling. Monachesi et al. (2020) analytically derived an exact expression for the effective fluid bulk modulus, valid for a patchy saturated two-layer hydraulically disconnected system with each layer filled with a different fluid.

Among other works dealing with two-phase fluid saturation in poroelastic media, we mention Qi et al. (2014) that used a membrane stiffness to model the effect of capillarity on wave propagation in patchy-saturated rocks. Also, Auriault et al. (1989) obtained the form of the dynamic equations for porous media saturated by two-phase fluids using homogenization techniques.

Here we use a FE procedure to determine the effective P-wave modulus of three periodic poroelastic layers saturated by two-phase fluids. Each layer can be saturated by gas-brine, oil-gas or oil-brine, thus this model is able to mimic the simultaneous presence of gas, oil and brine in hydrocarbon reservoirs.

The methodology consists of applying compressibility tests to a representative sample of the material and measure the resulting stress and strains, which quotient yields the desire P-wave modulus. The results are first compared with those of a FE method, presented and validated in Santos et al. (2009) and Santos and Savioli (2018), where the poroelastic matrix is saturated by a single-phase effective fluid. Then it is applied to several Cases of three-periodic samples with patchy gas-oil, gas-brine and brine-oil. The wetting phase can be either brine or oil, while the non-wetting phase can be either gas, oil or brine depending on the Case analyzed.

THE MATHEMATICAL MODEL

In a poroelastic medium saturated by a two-phase fluid, there is a solid phase, a wetting phase and a non-wetting one, indicated by the subindexes or superindexes s, w, n. Let S_w, S_n denote the wetting and non-wetting saturations, with S_{rw} and S_{rn} being the associated residual saturations. It is assumed that the two-phase fluid completely saturates the pore space, so that $S_w+S_n = 1$, with immobile wetting fluid in $[0, S_{rw}]$ and immobile non-wetting fluid in $[0, S_{rn}]$, and $S_{rw} > 0$.

Furthermore, we assume a funicular regime of flow, so that each fluid phase occupies continuous paths, where both fluids simultaneously flow. Then, we have

$$S_{rw} < S_w < 1 - S_{ro}, \quad S_{ro} < S_o < 1 - S_{rw}. \tag{1}$$

Let $\mathbf{u}^s$, $\widetilde{\mathbf{u}}^n$ and $\widetilde{\mathbf{u}}^w$ denote the time Fourier transforms of the averaged displacement vectors of the solid, non-wetting and wetting phases, respectively. Set

$$\mathbf{u}^\theta = \phi(\widetilde{\mathbf{u}}^\theta - \mathbf{u}^s),\ \xi^\theta = -\nabla \cdot \mathbf{u}^\theta,\ \theta = n, w, \quad \mathbf{u} = (\mathbf{u}^s, \mathbf{u}^n, \mathbf{u}^w), \tag{2}$$

where ϕ denote the matrix total porosity (i.e., the void space occupied for both immobile and mobile fluids). Let $\boldsymbol{\tau}(\mathbf{u})$ be the stress tensor of the bulk material and let us denote by $\mathcal{T}_n(\mathbf{u})$ and $\mathcal{T}_w(\mathbf{u})$ the generalized forces of the two-fluid phases.

The diffusion equations for a poroelastic medium saturated by a two-phase fluid are Santos et al. (1990a); Ravazzoli et al. (2003):

$$\nabla \cdot \boldsymbol{\tau}(\mathbf{u}) = 0, \tag{3}$$

$$i\omega\, d_n\, \mathbf{u}^n - i\omega\, d_{nw}\, \mathbf{u}^w + \nabla \mathcal{T}_n(\mathbf{u}) = 0, \tag{4}$$

$$i\omega\, d_w\, \mathbf{u}^w - i\omega\, d_{nw}\, \mathbf{u}^n + \nabla \mathcal{T}_w(\mathbf{u}) = 0. \tag{5}$$

The constitutive equations, with ε_{ij} denoting the strain tensor, are

$$\tau_{ij}(\mathbf{u}) = 2\mu\, \varepsilon_{ij} + \delta_{ij}(\lambda_u\, e^s - F_1\, \xi^n - F_2\, \xi^w), \tag{6}$$

$$\mathcal{T}_n(\mathbf{u}) = (S_n + \beta)P_n - \beta P_w = -F_1\, e^s + N_1\, \xi^n + N_3\, \xi^w, \tag{7}$$

$$\mathcal{T}_w(\mathbf{u}) = S_w\, P_w = -F_2\, e^s + N_3\, \xi^n + N_2\, \xi^w. \tag{8}$$

The coefficients in the constitutive equations 6 - 8, defining the generalized forces τ_{ij}, $\mathcal{T}_n$ and $\mathcal{T}_w$, are computed as follows (Santos et al., 1990a; Ravazzoli et al., 2003). The coefficient μ is the shear modulus of the dry rock and $K_u = 1/C_u = \lambda_u + (2/3)\mu$ is the undrained bulk modulus, determined by (Santos et al., 1990b)

$$K_u = K_s(K_m + \Xi)/(K_s + \Xi), \tag{9}$$

$$\Xi = K_f(K_m - K_s)/\phi(K_f - K_s), \tag{10}$$

$$K_f = \alpha\left(\gamma S_n C_n + S_w C_w\right)^{-1},\ \alpha = 1 + (S_n + \beta)(\gamma - 1), \tag{11}$$

$$\gamma = \left(1 + P'_{ca}(S_n) S_w C_w\right)\left(1 + P'_{ca}(S_n) S_n S_w C_n\right)^{-1}, \tag{12}$$

$$\beta = \frac{P_{ca}(S_n)}{P'_{ca}(S_n)}. \tag{13}$$

In equations 9-11, K_m, K_s, K_n and K_w are the bulk moduli of the dry matrix, grains and non-wetting and wetting fluids, respectively, with corresponding compressibilities $C_l = K_l^{-1}$, $l = m, s, n, w$. The other coefficients in equations 6- 8 can be obtained from the relations

$$F_1 = \chi K_u[(S_n + \beta)\gamma - \beta], \tag{14}$$

$$F_2 = \chi K_u S_w, \tag{15}$$

$$N_1 = -N_3 - F_1 C_m \delta^{-1}, \quad N_2 = r F_2 q^{-1}, \tag{16}$$

$$N_3 = -N_2 - F_2 C_m \delta^{-1}, \tag{17}$$

with

$$\chi = \left[\delta + \phi\left(C_m - C_u\right)\right]\left\{\alpha\left[\delta + \phi\left(C_m - C_f\right)\right]\right\}^{-1}, \quad \delta = C_s - C_m, \tag{18}$$

$$q = \phi\left(C_n + 1/P'_{ca}(S_n) S_n S_w\right), \tag{19}$$

$$r = (S_n + \beta)C_s + \left(C_c - C_m\right)\left[qB_2 + (S_n + \beta)\left(1 - C_s C_u^{-1}\right)\right]. \tag{20}$$

The viscous coupling coefficients d_n, d_w and d_{nw} in (4)-(5) are chosen of the form

$$d_l(\bar{S}_l) = (\bar{S}_l)^2 \frac{\eta_l}{\kappa K_{rl}(\bar{S}_l)}, \quad l = n, w, \tag{21}$$

$$d_{nw}(\bar{S}_n, \bar{S}_w) = \epsilon\left(d_n(\bar{S}_n) d_w(\bar{S}_w)\right), \tag{22}$$

where η_n, η_w are the fluid viscosities and κ, $K_{rn}(S_n), K_{rw}(S_w)$ are the absolute permeability and the relative permeability functions, respectively. Also, $d_{nw}(S_n, S_w)$ is a cross dissipative function (see Auriault et al. (1989)), with ϵ a small number to be chosen in the numerical experiments.

Harmonic experiment to determine the effective plane-wave modulus

Consider a reference square $\Omega = (0, L)^2$ in the (x, z)-plane containing a periodic sequence of three poroelastic layers saturated by a two-phase fluid. Let $\Gamma^L, \Gamma^B, \Gamma^R, \Gamma^T$ be the left, bottom, right and top boundaries of Ω, so that the boundary Γ of Ω is $\Gamma = \Gamma^L \cup \Gamma^B \cup \Gamma^R \cup \Gamma^T$. Let $\widetilde{\mathbf{u}}^s$ denote the macroscopic solid displacement vector in Ω and $\mathcal{T}(\widetilde{\mathbf{u}}^s)$, $\mathcal{E}(\widetilde{\mathbf{u}}^s)$ the time Fourier transforms of the macroscopic stress and strain tensors in Ω.

The constitutive equations of an effective viscoelastic medium long-wave equivalent to the fluid-saturated poroelastic medium Ω are

$$\mathcal{T}_{jk}(\widetilde{\mathbf{u}}^s) = \overline{\lambda}\nabla \cdot \widetilde{\mathbf{u}}^s \delta_{jk} + 2\overline{\mu}\mathcal{E}_{jk}(\widetilde{\mathbf{u}}^s). \tag{23}$$

The effective P-wave modulus $\overline{M}_u = \overline{\lambda} + 2\overline{\mu}$ can be determined by applying a compressibility time-harmonic test in the normal direction to the layering as follows. Let $\boldsymbol{\nu}$ the unit vector outer normal on Γ and $\boldsymbol{\chi}$ a unit vector tangent of Γ oriented counterclockwise. Then, we formulate the following boundary-value problem (BVP): solve equations 3-5 with the boundary conditions

$$\boldsymbol{\tau}(\mathbf{u})\nu \cdot \boldsymbol{\nu} = -\Delta P, \quad (x, z) \in \Gamma^T, \tag{24}$$

$$\boldsymbol{\tau}(\mathbf{u})\nu \cdot \boldsymbol{\chi} = 0, \quad (x, z) \in \Gamma, \tag{25}$$

$$\mathbf{u}^s \cdot \boldsymbol{\nu} = 0, \quad (x, z) \in \Gamma^L \cup \Gamma^R \cup \Gamma^B, \tag{26}$$

$$\mathbf{u}^n \cdot \boldsymbol{\nu} = 0, \quad \mathbf{u}^w \cdot \boldsymbol{\nu} = 0, \quad (x, z) \in \Gamma. \tag{27}$$

In this experiment, a uniform compression is applied on Γ^T, the solid is not allowed to move normally to the bottom and lateral boundaries and no tangential forces are applied on Γ. Interlayer flow occurs as the sample oscillates at a given frequency.

Note that the solution of this BVP satisfies the relations

$$\epsilon_{11}(\mathbf{u}^s) = \ \epsilon_{13}(\mathbf{u}^s) = \nabla \cdot \mathbf{u}^n = \nabla \cdot \mathbf{u}^w = 0. \tag{28}$$

Thus, $\mathcal{E}_{11}(\widetilde{\mathbf{u}}^s) = \mathcal{E}_{13}(\widetilde{\mathbf{u}}^s) = 0$ and equation 23 reduces to

$$\mathcal{T}_{33} = \overline{M_u}\mathcal{E}_{33}. \tag{29}$$

Now $\overline{M_u}$ can be determined from equation 29 by obtaining $\mathcal{T}_{33}$ and $\mathcal{E}_{33}$ as averages of the mesoscopic stress and strain tensors associated with the solid phase over the sample Ω, i.e.,

$$\mathcal{T}_{33} = \frac{1}{\Omega}\int_\Omega \tau_{33} d\Omega, \qquad \mathcal{E}_{33} = \frac{1}{\Omega}\int_\Omega \epsilon_{33} d\Omega. \tag{30}$$

The P-wave phase velocity $V_p(\omega)$ and quality factor $Q(\omega)$ of the periodic layered medium are obtained from the equations (Carcione, 2014)

$$V_p(\omega) = \left[\mathrm{Re}\left(\frac{1}{V_c(\omega)}\right)\right]^{-1}, \quad \frac{1}{Q(\omega)} = \frac{\mathrm{Im}(V_c(\omega)^2)}{\mathrm{Re}(V_c(\omega)^2)} \quad , \tag{31}$$

where $V_c(\omega)$ is the complex P-wave velocity

$$V_c(\omega) = \sqrt{\frac{\overline{M}_u(\omega)}{\overline{\rho_b}}}, \tag{32}$$

In equation 32, $\overline{\rho_b}$ is the bulk density, computed in terms of the grain density, ρ_s, and the non-wetting and wetting phases densities, ρ_n and ρ_w, as $\overline{\rho_b} = (1-\phi)\rho_s + \phi(S_n\rho_n + S_w\rho_w)$.

The approximate solution of equations 3-5, together with the boundary conditions 24-27, is obtained by using a FE procedure as follows. The domain Ω is partitioned by a uniform mesh of square cells of side length h. The x and z components of the displacement vector $\mathbf{u}^s$ are represented on each cell by bilinear polynomials in the variables x and z that are continuous along the edges of adjacent cells, the local degrees of freedom (DOF's) being the vertices of the cells, so that they are globally continuous. The relative fluid displacements

$\mathbf{u}^n, \mathbf{u}^w$ are represented as follows: the x-component of $\mathbf{u}^n$ is a polynomial locally linear in x and constant in z while the z-component is a polynomial locally constant in x and linear in z. Similarly for $\mathbf{u}^w$. Furthermore, continuity of the normal components of $\mathbf{u}^n$ and $\mathbf{u}^w$ is imposed across the internal interfaces of the computational mesh. The local DOF's are the values of the normal components of $\mathbf{u}^n$ and $\mathbf{u}^w$ at the mid points of the edges of the cells. The work in Santos et al. (2009) presents a priori error estimates for a similar boundary-value problem, but for the case of single-phase fluids. It is demonstrated that the error of the FE procedure is of order $h^{1/2}$ in the energy norm and of order h in the L^2-norm. The argument can be generalized to the case of two-phase fluids analyzed here.

NUMERICAL EXPERIMENTS

We consider a square sample and six periods, each consisting of three 20 cm layers saturated by a two-phase fluid. The sample is discretized using a 90×90 uniform mesh. The relative permeability and capillary pressure functions are defined as (Douglas et al., 1997; Ravazzoli et al., 2003):

$$K_{rn}(S_n) = \left(1 - (1 - S_n)/(1 - S_{rn})\right)^2, \tag{33}$$

$$K_{rw}(S_n) = \left(\left[1 - S_n - S_{rw}\right] / \left(1 - S_{rw}\right)\right)^2, \tag{34}$$

$$P_{ca}(S_n) = A\left(1/(S_n + S_{rw} - 1)^2 - S_{rn}^2/[S_n(1 - S_{rn} - S_{rw})]^2\right), \tag{35}$$

where A is the capillary pressure amplitude. In all examples $A = 30$ kPa, $S_{rn} = 0$ and the matrix and fluid properties are given in Tables 1 and 2, respectively.

Comparison with single-phase fluid saturation

We consider two Cases where the residual wetting saturation is $S_{rw} = 1\%$ and each period has three layers.

- Case 1: Layer 1: gas-brine saturation, 0.12 % gas , Layer 2: gas-brine saturation, 98 % gas, Layer 3: oil-brine saturation, 98 % oil, brine is the wetting phase in the three layers.
- Case 2: Layer 1: gas-brine saturation, 0.12 % gas , Layer 2: gas-brine saturation, 98 % gas, Layer 3: oil-gas saturation, 98 % oil, brine is the wetting phase in Layers 1 and 2, oil is the wetting phase in Layer 3.

Since the theory of Cavallini et al. (2017) for layered three-periodic poroelastic media holds for single-phase fluids, we compare the results of the FE procedure with those of an effective single-phase fluid using a Reuss average of the fluid bulk modulus and an arithmetic average of the densities and viscosities of each fluid phase, i.e.,

$$1/(K_f^*) = S_n/K_n + S_w/K_w, \quad \eta^* = S_n\eta_n + S_w\eta_w, \quad \rho_f^* = S_n\rho_n + S_w\rho_w.$$

The corresponding results in the next figures are labeled *single-phase model*. For a detailed description of harmonic numerical experiments when the poroelastic matrix is saturated by single-phase fluids, we refer to Santos et al. (2009) and Santos and Savioli (2018). For single-phase fluids, the approximate location of the relaxation peak is (Carcione, 2014)

$$f_r = \frac{8\kappa M E_m}{\pi\eta L^2 E_c} \tag{36}$$

where $M = \left[(\alpha - \phi)/K_s + \phi/K_f^*\right]^{-1}$, $\alpha = 1 - K_m/K_s$, $E_m = K_m + 4/3\mu$, $E_c = K_c + 4\mu/3$, $K_c = K_m + \alpha^2 M$, and L is the spatial period. Thus, as viscosity increases or permeability decreases, the attenuation peak moves to lower frequencies.

Figures 1 and 2 show the effective P-wave phase velocities and dissipation factors $(1000/Q)$ for Case 1 as a function of frequency. While the P-wave velocities are quite close for both models, two attenuation peaks are seen in Figure 2, as predicted by the theory for single-phase fluids in Cavallini et al. (2017). The higher peak for the two-phase model is shifted to higher frequencies as compared with that of the single-phase model. Also, according to equation 36, the lower and higher frequency attenuation peaks correspond to the presence of oil and gas, respectively.

Figures 3 and 4 show the results for Case 2. The P-wave phase velocities are in good agreement at lower frequencies, but above 1 Hz the two-phase fluid curve predicts higher velocities, on the order of 5 % at about 35 Hz. On the other hand, the two-phase model predicts higher attenuation with the attenuation peak located at lower frequencies compared to the single-phase model. More specifically, the attenuation peak for the two-phase model is located at 14 Hz with a Q value of approximately 10, while that of the single-phase model is seen at 50 Hz with a Q-value close to 11. In this case, only one attenuation peak is predicted for two-phase and single-phase fluids saturation.

Two-phase fluids and patchy saturation

To model quasi-fractal variations of gas, oil or brine saturation (patchy saturation), we use the von Karman autocorrelation function, whose 2D wave number-domain power spectrum

is (Frankel and Clayton, 1986; Santos et al., 2009; Santos and Gauzellino, 2017)

$$P(k_x, k_z) = (1 + k^2 \mathrm{a}^2)^{-(H+N_e/2)} \tag{37}$$

where $k = \sqrt{k_x^2 + k_z^2}$ is the wave-number, N_e is the Euclidean dimension, a is the correlation length and H is a self-similarity coefficient (the Hurst exponent, $0 < H < 1$). Equation 37 defines a fractal process of dimension $D = N_e + 1 - H$ at scales smaller than a. In the following examples $N_e = 2$, $D = 2.2$ and a approximately 0.5 % of the domain size. The generation of fractal patchy saturation is explained in detail in Santos et al. (2009); Santos and Gauzellino (2017).

A set of numerical examples consider the following Cases, with $S_{rw} = 10$ % and the wetting phase being either brine or oil depending on the cases defined below.

- Case 3: Brine is the wetting phase in the three layers. Layer 1: gas-brine saturation, 0.12 % gas. Layer 2: patchy gas-brine saturation, overall gas saturation is 10 % or 30 %. Layer 3: oil-brine saturation, 89 % oil.

- Case 4: Brine is the wetting phase in the three layers. Layer 1: gas-brine saturation, 0.12 % gas, Layer 2: patchy gas-brine saturation, overall gas saturation is 10 % or 30 %, Layer 3: patchy oil-brine saturation, overall oil saturation is 10 % or 30 %

- Case 5: Brine is the wetting phase in the three layers. Layer 1: gas-brine saturation, 0.12 % gas. Layer 2: gas-brine saturation, 89 % gas. Layer 3: patchy oil-brine saturation, overall oil saturation 10 % or 30 %.

- Case 6: Layer 1: gas-brine saturation, 0.12 % gas, brine is the wetting phase. Layer 2: patchy gas-oil saturation, oil is the wetting phase. Layer 3: patchy brine-oil saturation, oil is the wetting phase. Overall gas/brine saturations 10 % and 40 %.

Figures 5 and 6 display the phase velocity and dissipation factor for Case 3 and overall patchy gas-brine saturations of 10 % and 30 % in Layer 2. Figure 5 shows higher velocities for non-patchy than for patchy saturation (about 17 % higher) and quite similar velocities for both values of the overall gas saturation, except at higher frequencies, with values for 30% and 10 % patchy saturation below and above that of non-patchy saturation, respectively. Figure 6 shows two attenuation peaks for both overall saturations, which at lower frequencies are associated with the oil phase and at higher frequencies correspond to the gas phase. The peaks for non-patchy saturation for Case 1 are close each other, and located at lower frequencies compared to those of Case 1 in Figure 2. The difference between these two curves is due to the different values of saturations and residual oil and gas saturations.

Figures 7 and 8 display plots of the fluid pressure at 20 Hz for 10 % and 30 % overall gas saturation in Layer 2. We compute the fluid pressure as $\mathcal{T} = \mathcal{T}_n + \mathcal{T}_w$, with $\mathcal{T}_n, \mathcal{T}_w$ defined in equations 7-8. It can be seen that the gradients of fluid pressure in the Layer 2 region are much more noticeable at 10 % than at 30 % overall gas saturation, in agreement with Figure 6.

Figures 9 and 10 show the phase velocities and dissipation factors for Case 4. As in Case 3, the velocities for patchy saturations in Figure 9 are lower than those for non-patchy saturation, with maximum differences of about 25 %, and tend to reach values below and above the value for non-patchy saturation. Figure 10 predicts the existence of only one attenuation peak for the two values of overall gas and oil patchy saturation. Instead, the curve for Case 1 for non-patchy saturation shows two adjacent peaks of similar amplitude. In fact, a second attenuation peak for patchy saturation is found at very low frequencies, showing negligible attenuation; for brevity the figure is not included.

The results for Case 5 are presented in Figures 11 and 12. Velocities for Case 1 and the two values of overall oil (patchy) saturation are in good agreement for all frequencies. The dissipation factors exhibited in Figure 12 predict two attenuation peaks for non-patchy and 10 % overall oil (patchy) saturation. Furthermore, the 30 % overall oil saturation curve shows only one attenuation peak.

Finally, Figure 13 exhibit dissipation factors for the two-phase and single-phase models for Case 6. It can be observed two attenuation peaks for the two-phase model, much higher at low frequencies for the lowest overall patchy saturation (an expected result), while the single-phase model exhibits a single peak. Furthermore, the attenuation peak is wider as compared with the previous cases. These differences in attenuation are associated with the fact that in the two-phase model oil is the wetting phase in Layers 2 and 3. This assumption generates flow interactions between the two fluids via the relative permeability functions in a way that induces a second peak, an effect that is not predicted when using single-phase fluids.

DISCUSSION

The results show that the seismic response of thin layers reservoir rocks can give information about the subsurface when the properties of the saturant fluids are included in the study of the WIFF phenomenon.

In fact, the numerical experiments have shown that, in the frequency band, the amplitude and location of attenuation peaks as well as velocity dispersion of seismic waves may vary depending on whether brine or oil wets the pore space.

These results have important implications in the adquisition and interpretation of accu-

rate subsurface images when performing activities related to exploration or production of hydrocarbon reservoirs.

The additional parameters required for using the two-phase fluid model in upscaling numerical procedures are the capillary pressure and relative permeability functions. These data is either already available in geophysics and reservoir engineering literature as correlation equations or can be obtained from laboratory tests. The potential benefits are much greater than the cost of their inclusion in the implementation of numerical models.

CONCLUSIONS

We have presented a numerical procedure to obtain the seismic response of a periodic sequence of three poroelastic layers saturated by two-phase fluids. The technique consists of defining boundary-value problems associated with compressions normal to the layering, which are solved with a finite-element method. First, the case of non-patchy saturation is analyzed and then the methodology is applied to patchy saturation. The results for non-patchy saturation are compared with those obtained with effective single-phase fluids, for which an analytical solution exists. It is observed that the presence of capillary forces and the relative flow between the two fluids induce noticeable changes in phase velocity and attenuation of the P-wave when compared with single-phase fluids. Besides, the velocities predicted for non-patchy saturation are generally higher than those obtained for patchy saturation.

One additional and important factor in reservoir rocks saturated by two-phase fluids is wettability, i.e., the role of each fluid as wetting or non-wetting phase. In the numerical simulations, interchanging the roles of the wetting and non-wetting fluids, either two or one

attenuation peaks are obtained, a result that cannot be predicted by the Biot theory, valid for single-phase fluids. In summary, the simulations predict dispersion and attenuation effects in hydrocarbon reservoir rocks that cannot be described if single-phase fluids are used. The methodology presented here will be extended to the anisotropic case in a future work.

REFERENCES

Auriault, J. L., O. Lebaigue, and G. Bonnet, 1989. Dynamics of two immiscible fluids flowing through deformable porous media: Transport in Porous Media, **4**, 105–128.

Ba, J., W. Xu, L. Y. Fu, J. M. Carcione, and L. Zhang, 2017, Rock anelasticity due to patchy saturation and fabric heterogeneity: A double double-porosity model of wave propagation: Journal of Geophysical Research: Solid Earth, **122 (3)**, 1949–1976.

Barbosa, N. D., J. G. Rubino, E. Caspari, and K. Holliger, 2017, The sensitivity of seismic attenuation and phase velocity to intrinsic background anisotropy in fractured porous rocks: A numerical study: Journal of Geophysical Research: Solid Earth, **122(10)**, 8181–8199.

Biot, M. A., 1956a, Theory of propagation of elastic waves in a fluid-saturated porous solid. I. Low frequency range: Journal of the Acoustical Society of America, **28**, 168–178.

Biot, M. A., 1962, Mechanics of deformation and acoustic propagation in porous media, Journal of Applied Physics, **33**, 1482–1498.

Brooks, R.H., and A.T. Corey, 1964, Hydraulic Properties of Porous Media: Hydrology Papers, **No.3**, Colorado State U., Fort Collins, Colorado.

Carcione, J. M., 2014, Wave Fields in Real Media: Wave propagation in Anisotropic, Anelastic, Porous and Electromagnetic Media, 3rd ed., revised and extended: Elsevier, Amsterdam.

Carcione, J. M., F. Cavallini, J. E. Santos, C. L. Ravazzoli, and P. M. Gauzellino,2004, Wave propagation in partially-saturated porous media: Simulation of a second slow wave: Wave Motion, **39**, 227–240.

Cavallini, F., J. M. Carcione, D. Vidal de Ventos, and L. Engell-Sorensen, 2017, Low-frequency dispersion and attenuation in anisotropic partially saturated rocks: Geophysical

Journal International, **209**, no.3, 1572–1584, doi: 10.1093/gji/ggx107.

Chavent, G. and J. Jaffre, 1986, Mathematical Models and Finite elemnt Methods for Reservoir Simulation, North Holland.

Douglas, J., Jr., F. Furtado, and F. Pereira, 1997, On the numerical simulation of waterflooding of heterogeneous petroleum reservoirs: Comput. Geosci., **1**, 155–190.

Frankel, A., and R. W. Clayton, 1986, Finite difference simulation of seismic wave scattering: implications for the propagation of short period seismic waves in the crust and models of crustal heterogeneity: Journal of Geophysical Research, **91**, 6465–6489.

Hunziker, J., M. Favino, E. Caspari, B. Quintal, J. G. Rubino, R. Krause, and K. Holliger, 2018, Seismic attenuation and stiffness modulus dispersion in porous rocks containing stochastic fracture networks: Journal of Geophysical Research: Solid Earth, **123 (1)**, 125-143.

Li, K. and R. N. Horne, 2004, Universal capillary pressure and relative permeability model from fractal characterization of rock. In Twenty-Ninth Workshop on Geothermal Reservoir Engineering, Stanford University, California. **Vol. SGP-TR-75**.

Monachesi,L. B., U. Wollner, and J. Dvorkin, 2020, Effective Pore Fluid Bulk Modulus at Patchy Saturation: An Analytic Study: Journal of Geophysical Research: Solid Earth, **125**, e2019JB018267, https://doi.org/10.1029/2019JB018267.

Norris, A. N., 1993, Low-frequency dispersion and attenuation in partially saturated rocks: Journal of the Acoustical Society of America, **94**, 359–370, doi: 10.1121/1.407101.

Peaceman, D. W., Fundamentals of numerical reservoir simulation: Elsevier, Amsterdam.

Pride, S. R., J. G. Berryman, and J. M. Harris, 2004, Seismic attenuation due to wave-induced flow: Journal of Geophysical Research: Solid Earth, **109(B1)**.

Qi, Q., T. Müller, B. Gurevich, S. Lopes, M. Lebedev, and E. Caspari, 2014, Quantifying the

effect of capillarity on attenuation and dispersion in patchy-saturated rocks: Geophysics, **79**, WB35–WB50.

Ravazzoli, C. L., J. E. Santos, and J. M. Carcione, 2003, Acoustic and mechanical response of reservoir rocks under variable saturation and effective pressure: Journal of the Acoustical Society of America, **113**, 1801–1811.

Rozhko, A. Y., 2019, Bulk moduli and seismic attenuation in partially saturated rocks: hysteresis of liquid bridges effect: Geophysical Prospecting, **67(5)**, 1404-1430.

Rozhko, A. Y.,2020, Effective fluid bulk modulus in the partially saturated rock and the amplitude dispersion effects: Journal of Geophysical Research: Solid Earth, **125(3)**, e2019JB018693.

Santos, J. E. and P. M. Gauzellino, 2017, Numerical simulation in applied geophysics: Birkhauser, Lecture Notes in Geosystems Mathematics and Computing.

Santos, J. E., and G. B. Savioli, 2018, Long-wave equivalent viscoelastic solids for porous rocks saturated by two-phase fluids: Geophysical Journal International, **214**, 302–314.

Santos, J. E., J. Douglas Jr., J. M. Corberó, and O. M. Lovera, 1990a, A model for wave propagation in a porous medium saturated by a two–phase fluid: Journal of the Acoustical Society of America, **87**, 1439-1448.

Santos, J. E., J. Douglas Jr., and J. M. Corberó, 1990b, Static and dynamic behaviour of a porous solid saturated by a two-phase fluid: Journal of the Acoustical Society of America, **87**, 1428-1438.

Santos, J. E., C. L. Ravazzoli, P. M. Gauzellino, and J. M. Carcione, 2009, A numerical upscaling procedure to estimate effective bulk and shear moduli in heterogeneous fluid-saturated porous media: Computer Methods in Applied Mechanics and Engineering, **198**, 2067–2077.

Scheidegger, A. E., 1974, The physics of flow through porous media: University of Toronto, Toronto.

White, J. E., N. G. Mikhaylova, and F. M. Lyakhovitskiy, 1975, Low-frequency seismic waves in fluid-saturated layered rocks. In: Izvestija Academy of Sciences USSR, Physics Solid Earth, **10**, 654–659.

Wollner, U., and J. Dvorkin, 2016, Effective fluid and grain bulk moduli for heterogeneous thinly layered poroelastic media: Geophysics, **81 (6)**, D573–D584.

Wollner, U., and J. Dvorkin, 2018, Seismic-scale dependence of the effective bulk modulus of pore fluid upon water saturation: Geophysics, **83 (2)**, MR81–MR91.

TABLES

Table 1. Properties of the sandstone

Grain bulk modulus, K_s	33.4 GPa
density, ρ_s	2650 kg/m^3
Dry-matrix bulk modulus, K_m	1.3 GPa
shear modulus, μ	1.4 GPa
porosity, ϕ	0.3
permeability, κ	10^{-12} m^2

Table 2. Properties of the saturant fluids

Brine bulk modulus, K_w	2.2 GPa
density, ρ_w	975 kg/cm^3
viscosity, η_w	0.001 Pa $\cdot$ s
Oil bulk modulus, K_o	2 GPa
density, ρ_o	870 kg/cm^3
viscosity, η_o	0.3 Pa $\cdot$ s
Gas bulk modulus, K_g	0.0044515 GPa
density, ρ_g	42.316 kg/m^3
viscosity, η_g	1.1186 $\times 10^{-5}$ Pa $\cdot$ s

LIST OF FIGURES

Figure 12. P-wave dissipation factor as a function of frequency for the two-phase model for Cases 1 and 5. Overall oil saturations in Layer 3 are 10 % and 30 %.

Figure 13. P-wave dissipation factor as a function of frequency for the two-phase and single-phase models for case 6. Overall gas/brine saturations are 10 % and 40 %.

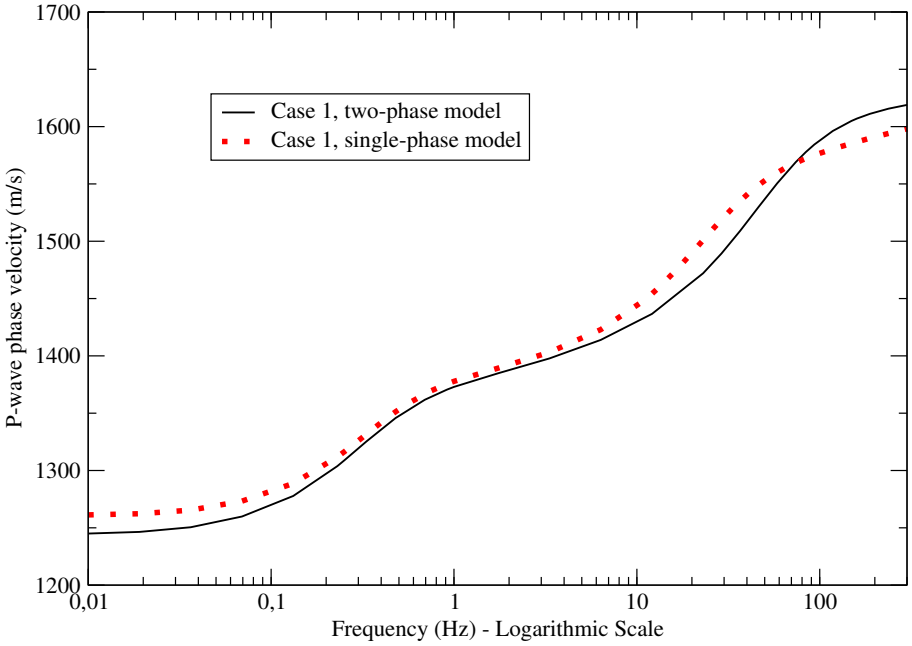

Figure 1: P-wave phase velocity as a function of frequency for the two-phase and single-phase fluid models. Case 1.

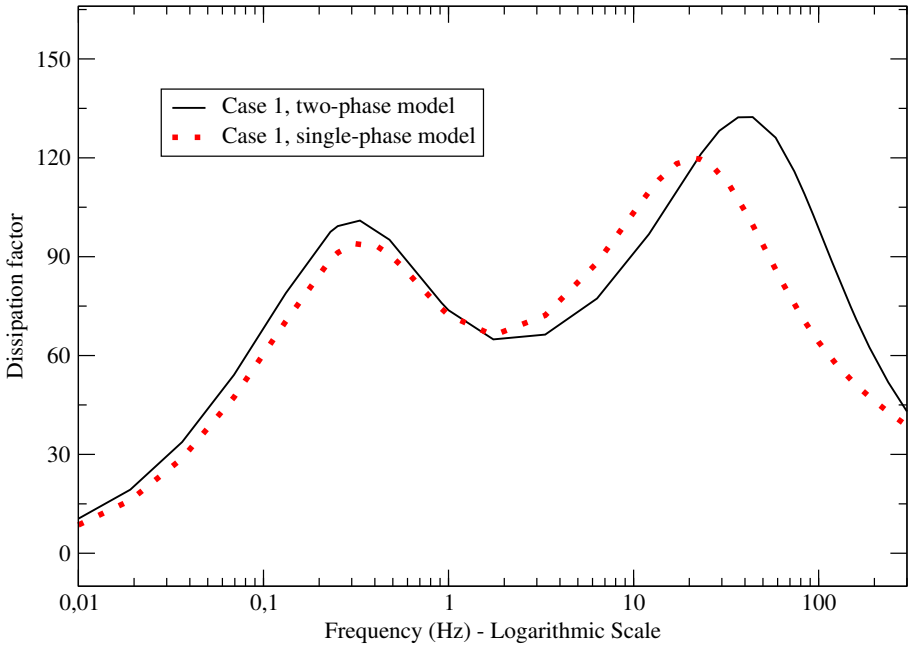

Figure 2: P-wave dissipation factor as a function of frequency for the two-phase and single-phase fluid models. Case 1.

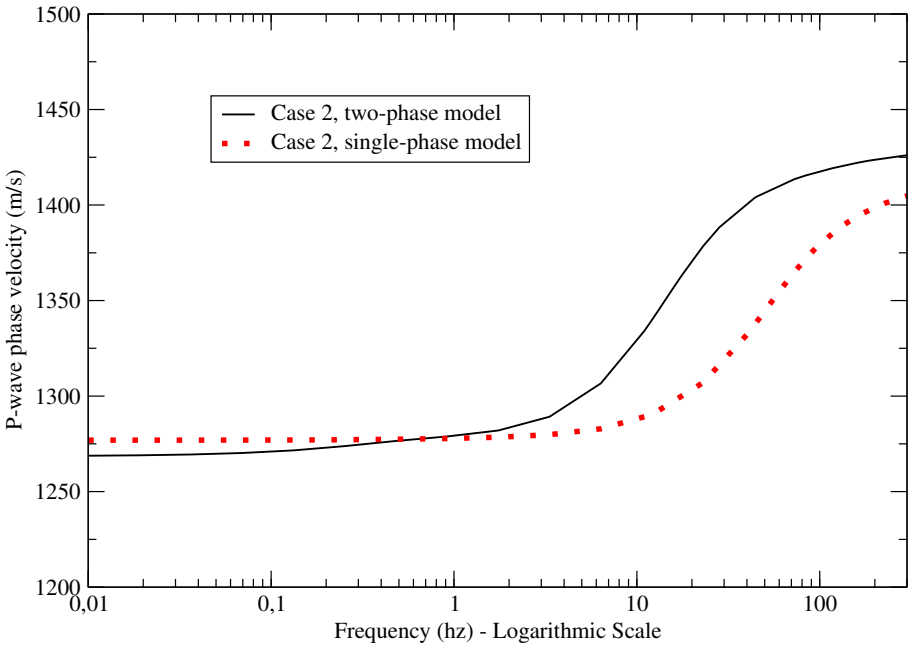

Figure 3: P-wave phase velocity as a function of frequency for the two-phase and single-phase fluid models. Case 2.

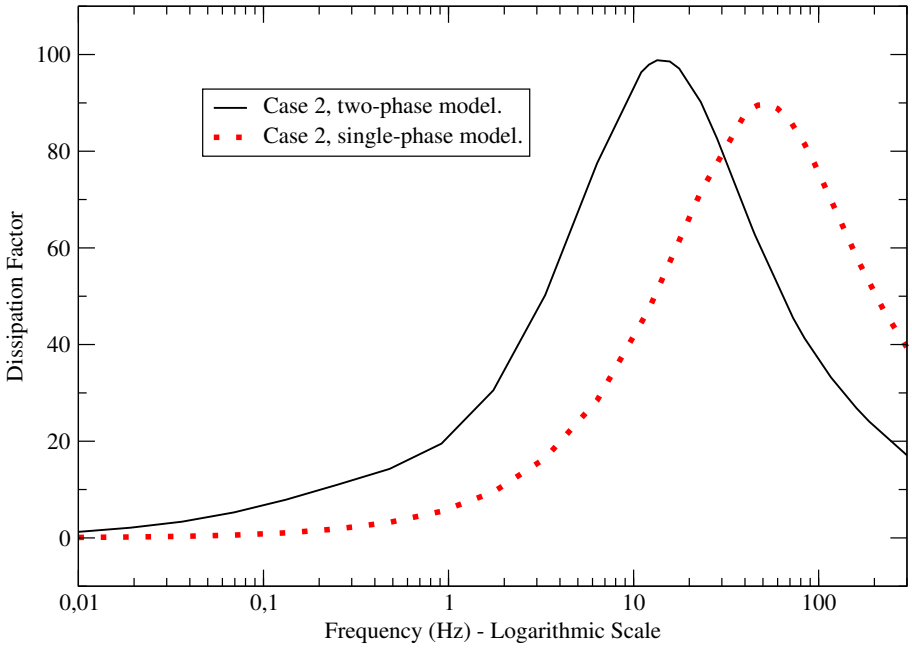

Figure 4: P-wave phase dissipation factor as a function of frequency for the two-phase and single-phase fluid models. Case 2.

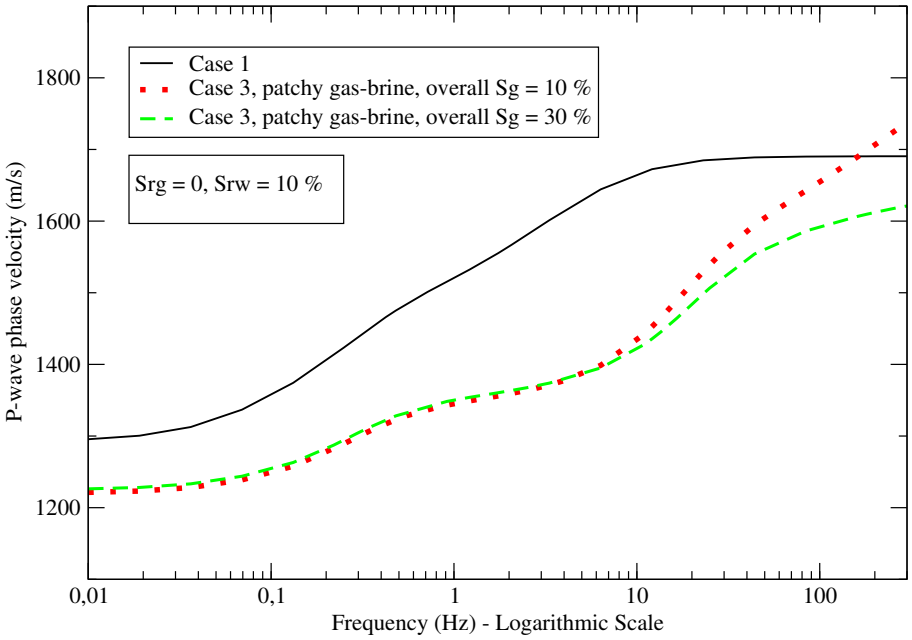

Figure 5: P-wave phase velocity as a function of frequency for the two-phase model for Cases 1 and 3. Overall gas saturations in Layer 2 are 10 % and 30 %.

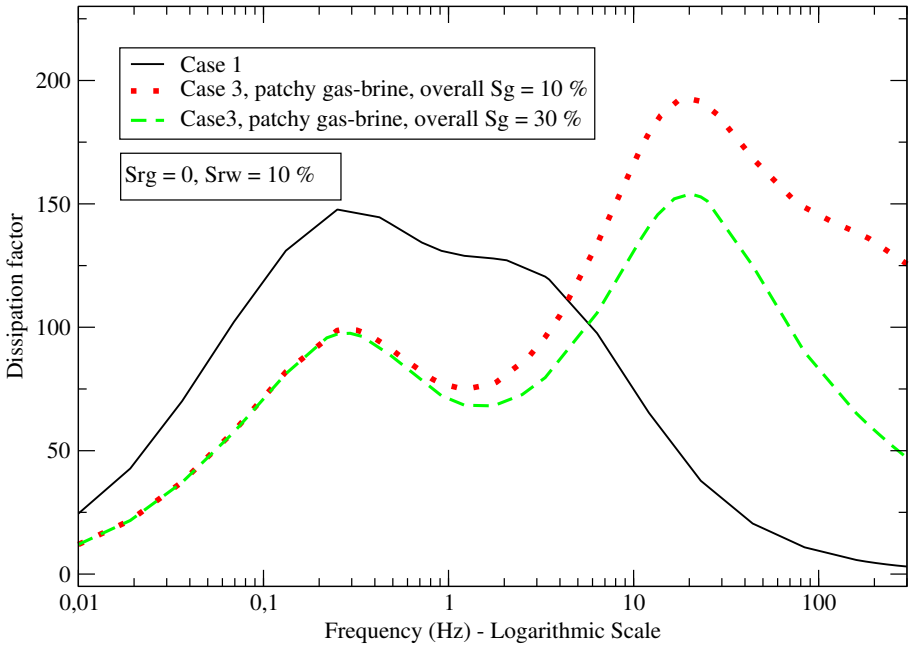

Figure 6: P-wave dissipation factor as a function of frequency for the two-phase model for Cases 1 and 3. Overall gas saturations in Layer 2 are 10 % and 30 %.

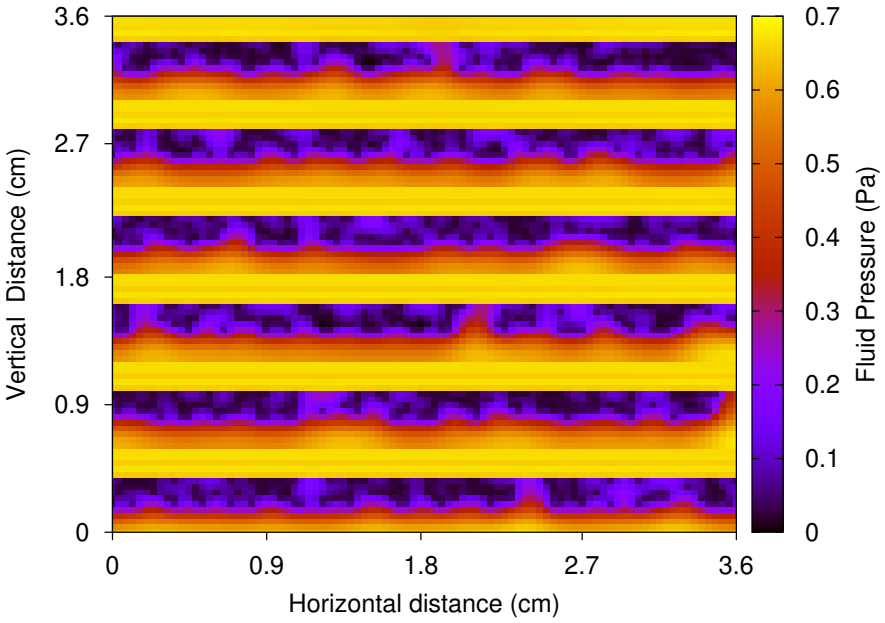

Figure 7: Fluid pressure at 20 Hz for Case 3. Overall gas saturation in Layer 2 is 10 %.

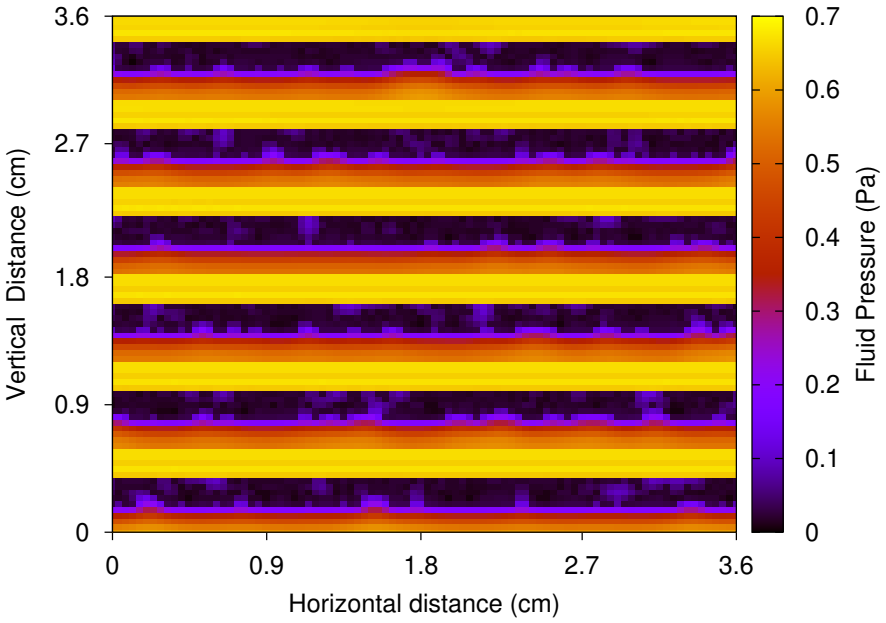

Figure 8: Fluid pressure at 20 Hz Case 3. Overall gas saturation in Layer 2 is 30 %.

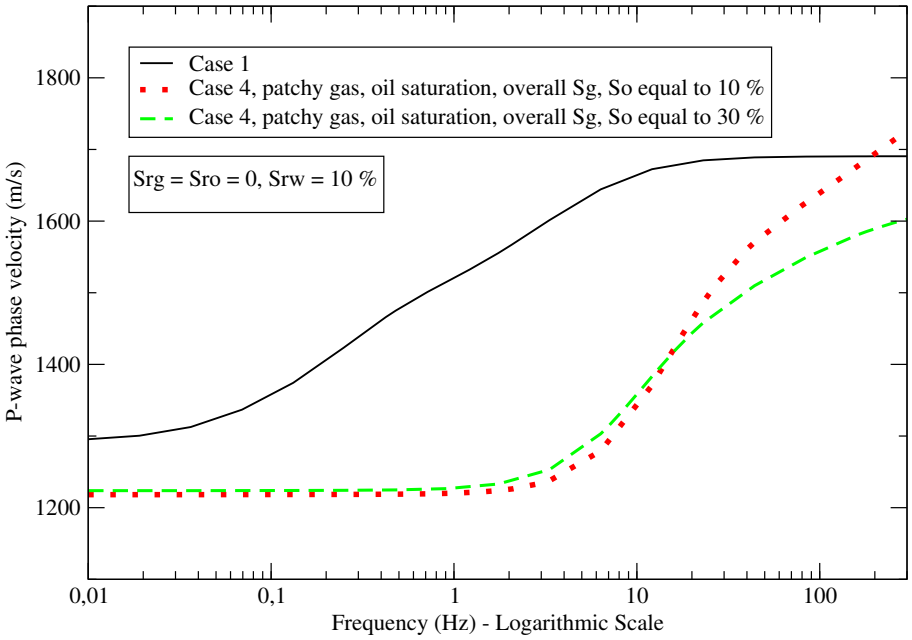

Figure 9: P-wave phase velocity as a function of frequency for the two-phase model for Cases 1 and 4. Overall gas/oil saturations are 10 % and 30 %.

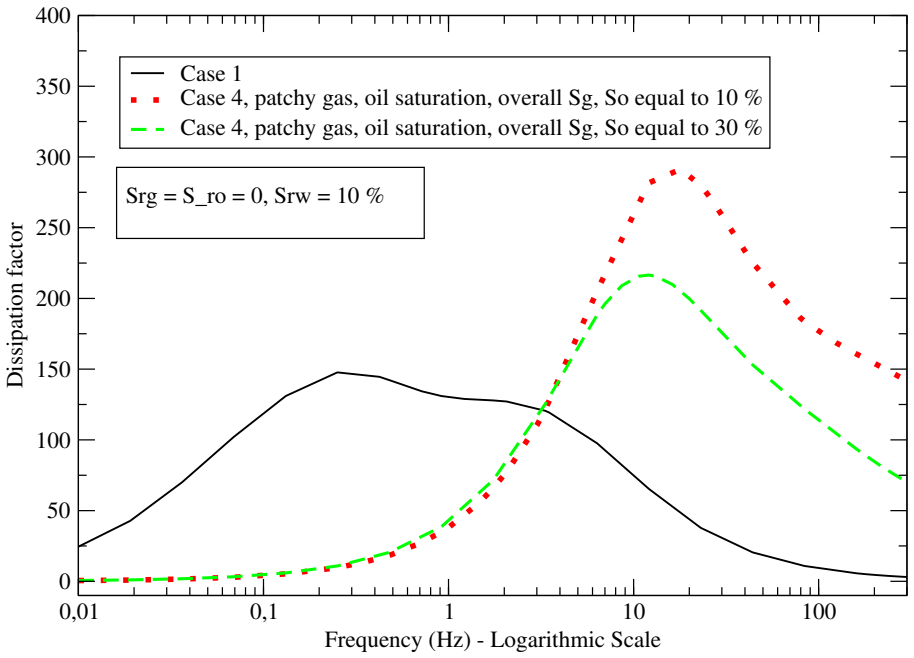

Figure 10: P-wave dissipation factor as a function of frequency for the two-phase model for Cases 1 and 4. Overall gas/oil saturations are 10 % and 30 %.

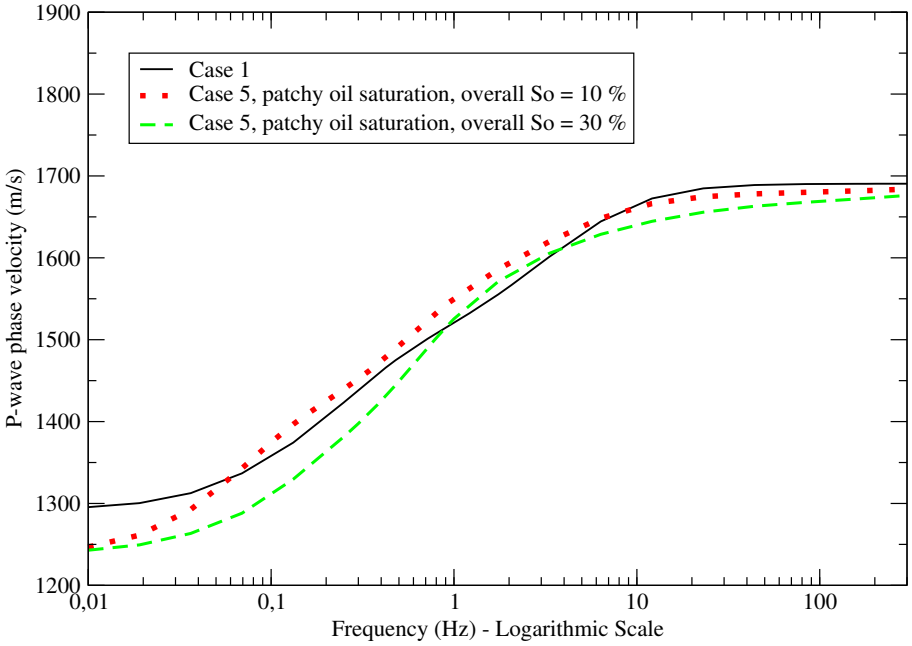

Figure 11: P-wave phase velocity as a function of frequency for the two-phase model for Cases 1 and 5. Overall oil saturations in Layer 3 are 10 % and 30 %.

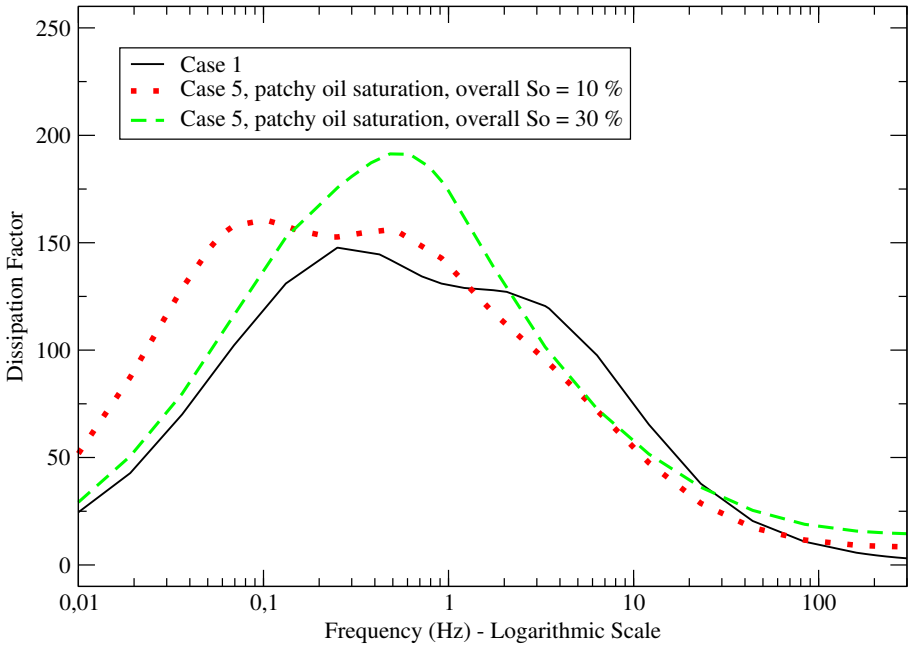

Figure 12: P-wave dissipation factor as a function of frequency for the two-phase model for Cases 1 and 5. Overall oil saturations in Layer 3 are 10 % and 30 %.

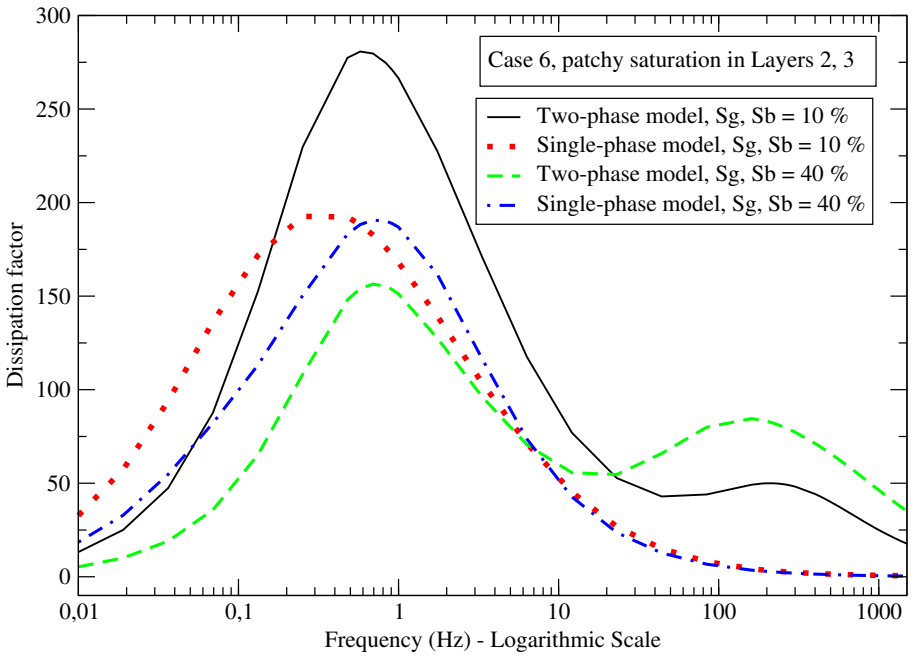

Figure 13: P-wave dissipation factor as a function of frequency for the two-phase and single-phase models for case 6. Overall gas/brine saturations are 10 % and 40 %.